Interpretation of Photocurrent Transients at Semiconductor Electrodes: Effects of Band-Edge Unpinning

Laurence M Peter[1], Alison B Walker[2], Thomas Bein[3], Alexander G Hufnagel[3,4] and Ilina Kondofersky[3,5]*

1. Department of Chemistry, University of Bath, Bath BA2 7AY, United Kingdom
2. Department of Physics, University of Bath, Bath BA2 7AY, United Kingdom
3. Department of Chemistry and Center for Nanoscience (CeNS), University of Munich (LMU), Butenandtstrasse 5-13, 81377 Munich, Germany
4. Current address: BASF SE, Carl Bosch Strasse 38, 67056 Ludwigshafen, Germany
5. Current address OHB System AG, Wolfratshauser Strasse 48, 81379 Munich, Germany

* corresponding author: l.m.peter@bath.ac.uk

Abstract

The transient photocurrent response of semiconductor electrodes to chopped illumination often shows spikes and overshoots that are usually interpreted as evidence that surface recombination is occurring. In the case of the high intensities used for light-driven water splitting, the interpretation is less straightforward since the electron transfer reactions are so slow that the minority carrier concentration at or near the surface increases to high values that modify the potential drop across the Helmholtz layer in the electrolyte, leading to 'band edge unpinning'. In addition, changes in chemical composition of the surface or local changes in pH may also alter the potential distribution across the semiconductor/electrolyte junction. A quantitative theory of band edge unpinning due to minority carrier build up is presented, and numerical calculations of transient photocurrent responses are compared with experimental examples for n-type Fe_2O_3 and p-type lithium-doped CuO electrodes. It is shown that the apparently high reaction orders (up to third order) with respect to hole concentration reported for hematite photoanodes can be explained as arising from an acceleration of hole transfer by the increased voltage drop across the Helmholtz layer associated with band edge unpinning. The limitations of the band edge unpinning model are discussed considering additional effects associated with modification of the potential distribution brought about by light-induced changes in surface composition, surface dipoles and surface ionic charge.

~

1. Introduction

Interest in semiconductor photoelectrochemistry has been rekindled in recent years by the prospect of being able to generate solar fuels by photoelectrolysis of water or photoelectrochemical reduction of carbon dioxide, and many semiconductor materials have been investigated as potential photoanodes or photocathodes. Key issues are chemical stability, appropriate alignment of the semiconductor bands with the hydrogen and oxygen redox Fermi levels, efficient light harvesting and low recombination losses. Recombination losses are particularly problematic in the photoelectrolysis of water since the half reactions involve multiple electron/proton transfer steps, some with high activation energies. Since the overall rate constants for the oxidation or reduction of water by photogenerated minority carriers are remarkable low, minority carriers build up at or near the surface where they have a high probability of being lost by recombination with majority carriers. This process can be mediated by surface states (surface electron-hole recombination[1-3]) or occur in the space charge region near the surface ('near-surface recombination[4]). Over the last 30 years, the competition between charge transfer and surface recombination has been studied extensively by intensity-modulated photocurrent spectroscopy (IMPS[5]), but it has proved difficult to derive definitive mechanistic information from the results. For this reason, alternative methods are needed to gain better insight into light-driven water splitting reactions.

The build-up and decay of the minority carrier concentration near (or at) the photoelectrode surface under illumination can be detected by methods such as microwave reflectivity[6, 7], optical absorption[8-10] and photocapacitance.[7,11,12] More commonly however, the effective lifetime of carriers at the surface is deduced from the photocurrent response to chopped illumination. Typically, in the photocurrent onset region, photocurrent transients for photoanode materials such as hematite (α-Fe_2O_3) exhibit the decay and negative overshoot shown in Figure 1 rather than a simple rectangular "on-off" response.

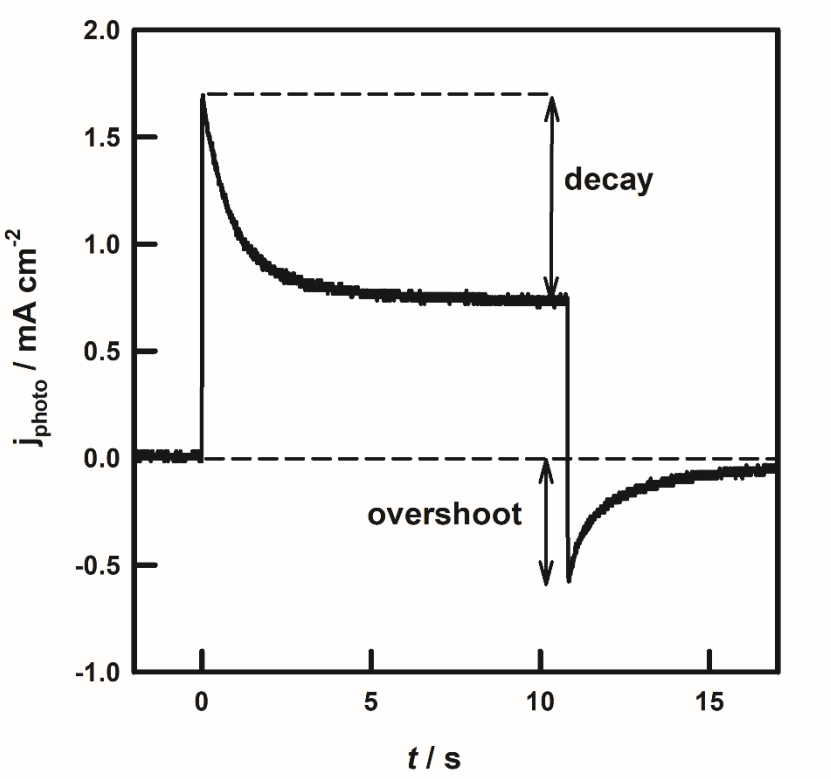

Figure 1. Transient photocurrent response of an α-Fe_2O_3 electrode in 1.0 M NaOH at 1.1 V vs. RHE showing the typical decay and overshoot interpreted as evidence of surface electron-hole recombination.[13, 14] However, note that the 'decay' is significantly larger than the 'overshoot'. Incident photon flux (455 nm) 1.1 $\times 10^{17}$ cm^{-2} s^{-1}. Film prepared by AACVD on FTO using ferrocene as precursor.[15]

Two further examples of transient photocurrent responses are shown in Figures 2 and 3 (see Appendix B for details of the preparation and characterization of these photoelectrodes).

Figure 2 shows the transient photocurrent response for an ultrathin (14 nm) ALD layer of hematite on FTO that has been annealed at 600^{o}C.[16] The decay and overshoot are again evident, but in this case the risetime of the 'on' spike is considerably longer than that of the 'off' spike. Closer examination shows that the time constant for the rising part of the 'on' transient is 15 ms, which is much higher than the RC time constant of the system, which is more than an order of magnitude smaller. The RC time constant corresponds to the charging of the space charge capacitance through the series resistance of the electrode and electrolyte. It can become a problem is the series resistance is high (e.g. if using conducting glass substrates) or if the electrode capacitance is high (rough surfaces or high doping). The negative 'off' transient, on the other hand, is much sharper with a rise time of around 400 μs. By contrast,

the rise and fall times for the AACVD hematite film (Figure 1) are both around 3 ms, in good agreement with the RC time constant measured by IMPS.[14]

The final experimental example shown in Figure 3 is for p-type $Li_xCu_{1-x}O$ (x = 0.013)[17], an oxide has stimulated interest as a potential photocathode material.[18] In this case, the cathodic photocurrent decays after the initial spike, but there is only a small overshoot. The magnitude of the current response declines with successive pulses. The objective of the present paper is to examine possible explanations for the types of transient response illustrated by Figures 1 to 3.

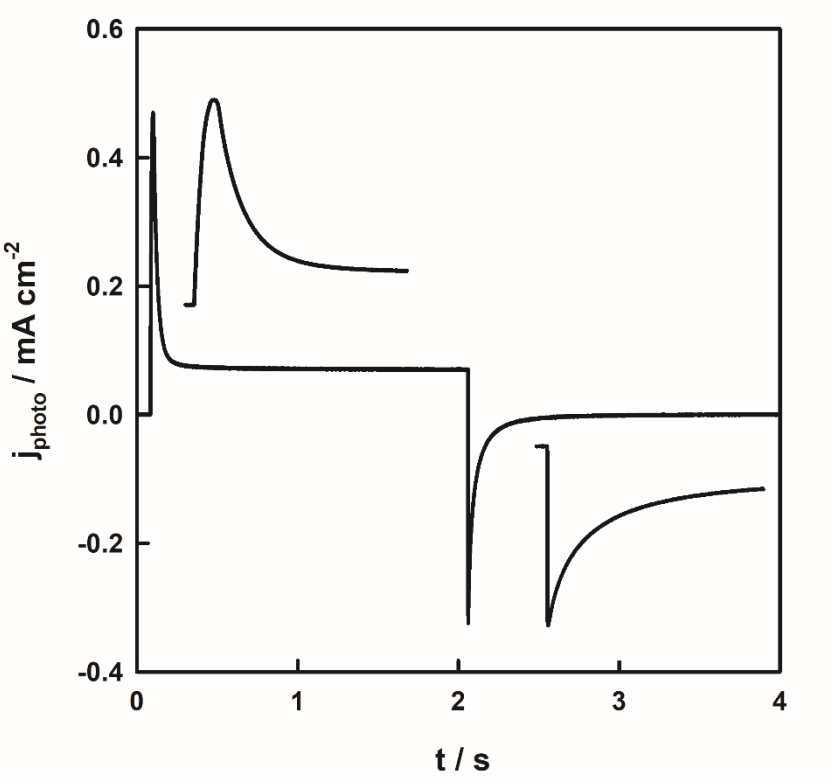

Figure 2. Photocurrent transient for 14 nm film of n-type hematite deposited on FTO-coated glass substrate (Pilkington 7 Ω square) by ALD using ferrocene as precursor and annealed at 600ºC.[16] Electrolyte 0.1 M NaOH. Potential 1.2 V vs RHE ($E - E_{fb}$ ca. 0.9 V) Incident photon flux (455 nm) 10^{17} cm^{-2} s^{-1}. The insets contrast the on and off spikes on an expanded time scale to show the slow rise of the on transient.

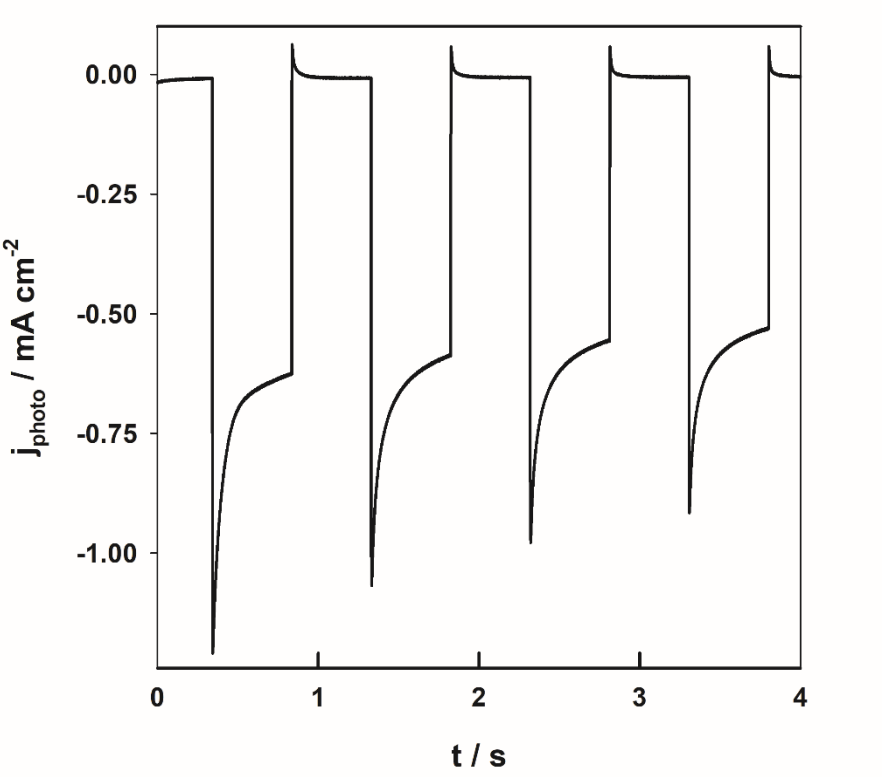

Figure 3. Transient photocurrent response of a $Li_xCu_{1-x}O$ photocathode (x = 0.013)[17]. Potential 0.41 V vs RHE ($E - E_{fb}$ ca. -1.1 V). Electrolyte 0.1 M Na_2SO_4. Incident photon flux (455 nm) 10^{17} cm^{-2} s^{-1}. Note the decline in the 'instantaneous' cathodic photocurrent spikes for successive pulses.

We have previously explained the transient photocurrent response of semiconductor photoelectrodes as follows.[5, 19] The 'instantaneous' photocurrent observed when the light is switched on corresponds to rapid separation of photogenerated electron hole pairs that takes place in the space charge region, with - for an n-type photoanode - holes moving to the interface to charge the space charge capacitance and electrons passing to the external circuit. In practice, the rise time of the 'on' spike is finite because it is determined by the RC time constant of the system, which is typically less than 1 ms for the kind of samples studied here. The subsequent photocurrent decay is then attributed to the build-up of photogenerated minority carriers (holes in this example) at or near the interface which causes an increasing flow of electrons (i.e. a negative current) into the surface due to recombination. After some time, a steady state is reached in which the rate at which holes reach the interface is exactly balanced by the rate at which they are consumed by charge transfer and recombination, and therefore the photocurrent becomes constant and equal to the current passing across the semiconductor/electrolyte

interface. The negative overshoot seen when the light is switched off arises because the hole flux is interrupted abruptly, revealing just the electron flux, which decays until all excess holes have been consumed by recombination and charge transfer, and the current returns to zero.

It follows from this explanation that the decrease in photocurrent up to the point at which the light is switched off (shown as 'decay' in Figure 1) should be equal in magnitude as the instantaneous negative spike ('overshoot' in Figure 1) since both measure the recombination current. However, in this example of the photocurrent response of a hematite electrode under intense illumination (roughly equivalent to 1 sun), this is evidently not the case. The negative spike is clearly smaller in magnitude than the decrease in current in the on period, so that some additional factor(s) besides recombination must be involved in the decay of the photocurrent after the initial spike. The most obvious explanation is that the build-up of holes at the interface modifies the potential distribution across the semiconductor electrolyte junction, increasing ΔV_H, the potential drop across the Helmholtz layer and decreasing $\Delta\phi_{SCR}$, the potential drop across the space charge region.

Since the applied potential relative to the flatband potential is equal to the sum of the potential drops across the space charge region and the Helmholtz region, any increase in ΔV_H due to the build-up of charge must be matched by a corresponding decrease in band bending and hence of the photocurrent. We refer to this phenomenon as *light-induced band edge unpinning*,[20] since the change in ΔV_H alters the alignment of the bands with respect to a reference redox level in the electrolyte.

The consequences of light-induced band edge unpinning have been explored quantitatively for methods involving small amplitude sinusoidal perturbation of the electrode potential (photoelectrochemical impedance spectroscopy[21]: PEIS) or illumination (intensity modulated photocurrent spectroscopy: IMPS[22]). However, the implications of band edge unpinning for attempts to determine the kinetics of charge transfer and recombination using

large amplitude "on-off" light steps have not been treated in any detail. Here we develop a relatively simple quantitative model that allows us to calculate the transient photocurrent response to periodic on-off illumination. The results show that the symmetry between the on and off transient spikes is lost when band edge unpinning occurs. In extreme cases at high band bending, the photocurrent may decay when the light is switched on but not show any overshoot when the light is switched off. We also consider other processes that may cause light-induced band edge unpinning in the context of water photoelectrolysis.

2. Modelling Band-Edge Unpinning in Terms of Minority Carrier Build-Up

We start by revisiting the simple model that we have used previously to describe the transient and periodic response of bulk (i.e. not nanostructured) photoelectrodes to small amplitude square wave or sinusoidal perturbations of light intensity or applied potential. We assume that absorption of photons creates electron-hole pairs that are separated by drift/diffusion. The solution of the generation collection value problem by Gärtner[23] gives the flux of minority carriers into the interface region as (derivation for a n-type photoanode: see Appendix A for Glossary of symbols).

$$J_G = I_0 \left[1 - \frac{exp(-\alpha(\lambda)W_{scr})}{1+\alpha(\lambda)L_p}\right] \quad 1)$$

where W_{scr}, the width of the space charge region (SCR), is given by

$$W_{scr} = \left(\frac{2\Delta\phi_{scr}\epsilon_r\epsilon_0}{qN_d}\right)^{1/2} \quad 2)$$

It is important to stress that equation 1 applies to a reasonably planar electrode. In the case of nanostructured electrodes, the separation of electron hole pairs involves the movement of minority carriers over short distances to the large internal surface area of the layer (for a recent discussion see ref.[24]). Here we limit the initial discussion to the case of reasonably planar photoelectrodes but note that the same general approach is possible for microstructured electrodes, although the hole flux term – equation 1- needs to be modified.

The time-dependent surface concentration of holes (p_{surf}, expressed as number per unit area) is determined by the rate of their arrival (i.e. the flux J_G predicted by the Gärtner equation) and the rate of their removal at the interface by charge transfer (first-order rate constant k_t) and recombination (first-order rate constant k_t).

$$\frac{dp_{surf}}{dt} = J_G - (k_t + k_r)p_{surf} \quad 3)$$

When the illumination is interrupted, equation 3 still applies with $J_G = 0$.

We note here that the formulation of equation 3 assumes that the rate of the photoelectrochemical process is first order in hole concentration. In the case of hematite and bismuth vanadate it has been reported that the rate of oxidation of water becomes third order in surface hole concentration at high intensities.[25, 26] However, as we show below, the apparent reaction order of 3 reported by Le Formal et al.[25] for light-driven water oxidation on hematite is probably an artefact arising from band edge unpinning.

If J_G, k_t and k_r are independent of p_{surf} and the charge transfer rate is first order in surface hole concentration, equation 3 is a simple first order linear differential equation with constant coefficients that is readily solved analytically to give the time dependence of the surface hole concentration. For a square illumination pulse of duration τ, the on and off parts of the transient hole concentration in the absence of band edge unpinning are

$$p_{surf}(t \leq \tau) = p_{surf}(\infty)\left(1 - e^{-(k_t+k_r)t}\right) \quad 4a)$$

$$p_{surf}(t \geq \tau) = p_{surf}(\tau)e^{-(k_t+k_r)} \quad 4b)$$

where the steady state surface hole concentration is given by

$$p_{surf,ss} = \frac{J_G}{k_t+k_r} \quad 5)$$

The symmetrical build up and decay of the surface hole density is illustrated in Figure 4. Note that the time axis is normalised as the dimensionless product $(k_t + k_r)t$, and the hole

concentration axis has been normalized by dividing by the steady state hole concentration. The time constant for the symmetrical build-up and decay is given by $(k_t + k_r)^{-1}$.

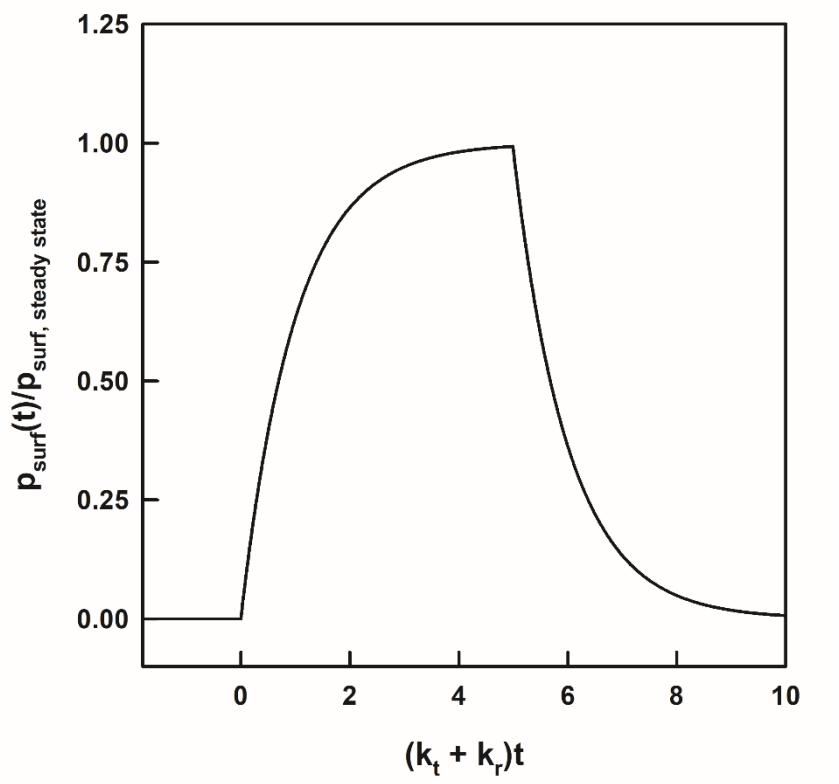

Figure 4. Plot showing the symmetrical build-up and decay of the surface hole concentration predicted by equation 4. The time and concentration axes have both been normalized as indicated. The time constant for the symmetrical build-up and decay is $(k_t + k_r)^{-1}$.

Since there is some confusion in the literature about what current is measured in the external circuit under transient conditions, we now examine the current densities associated with four processes: 1) the flow of holes into the interface, 2) charging of the space charge capacitance, 3) charge transfer across the interface and 4) the flow of electrons into the surface due to surface recombination.

Equation 3 can be rewritten in terms of current densities (rather than carrier fluxes) as

$$q\frac{dp_{surf}}{dt} = qJ_G - qk_t p_{surf} - qk_t p_{surf} \qquad 6a)$$

We can now identify the individual terms in equation 6a. The change in surface hole concentration with time corresponds to charging of the space charge capacitance (or when p_{surf}

decreases with time during the off period of the transient, to discharging). Equation 6a is therefore equivalent to

$$j_{charging} = j_{hole} - j_{transfer} + j_{recombination} \quad \text{6b)}$$

Note that here the hole current and transfer current both have a positive sign, whereas the recombination current has a negative sign since it corresponds to a flow of negatively charged electrons into the interface, i.e.

$$j_{recombination} = -qk_r p_{surf} \quad \text{6c)}$$

The net current density measured at any time is equal to the sum of the (positive) hole current density and the (negative) recombination current density, i.e.

$$j_{photo}(t) = j_{hole} + j_{recombination} = j_{charging} + j_{transfer} \quad \text{6d)}$$

This shows that the current measured in the external circuit at any instant during a photocurrent transient is not equal to the current transferred across the interface. There is also a charging component associated with the time dependence of the hole concentration at the surface. The measured current only becomes equal to the transfer current when the photocurrent decays to its steady state value $j_{photo}(\infty)$ and the charging current vanishes ($\frac{dp_{surf}}{dt} = 0$).

Note that during the off period, j_{hole} is zero ($J_G = 0$), so that

$$j_{photo}(t \geq \tau) = j_{recombination} = j_{charging} + j_{transfer} \quad \text{6e)}$$

giving a negative overshoot.

The time-dependent current for the on transient is best defined as the difference between the time-dependent photocurrent and the steady state photocurrent.

$$0 \leq t \leq \tau\text{: } j_{photo}(t) - j_{photo}(\infty) = +qJ_g \frac{k_r}{k_t + k_r}[exp - (k_t + k_r)t] \quad \text{7a)}$$

where the steady-state photocurrent is given by

$$j_{photo}(\infty) = qJ_G \left(\frac{k_t}{k_t + k_r}\right) = \eta_{ct} qJ_G \quad \text{7b)}$$

Here η_{ct} is the charge transfer efficiency, i.e. the fraction of holes arriving at the surface that are successfully used to oxidize species in the electrolyte.

When the light is switched off, the hole current vanishes almost instantaneously leaving only the recombination current, which at the switching time τ is given by

$$j_{rec}(\tau) = -qk_r p_{surf}(\tau) = -qk_r p_{surf}(\infty)\left(1 - e^{-(k_t+k_r)\tau}\right) = -q\frac{J_G k_r}{k_t+k_r}\left(1 - e^{-(k_t+k_r)\tau}\right) \quad 7c)$$

The off transient (negative overshoot) is given by

$$t \geq \tau: \quad j_{photo}(t \geq \tau) = -q\frac{J_G k_r}{k_t+k_r}\left(1 - e^{-(k_t+k_r)\tau}\right)e^{-(k_t+k_r)(t-\tau)} \quad 7d)$$

Figure 5 illustrates the normalized photocurrent response predicted by equation 7 for the case that η_{trans} = 0.3, i.e. $k_t/(k_t + k_r)$ = 0.3. The figure also shows the positive hole current and the negative recombination current.

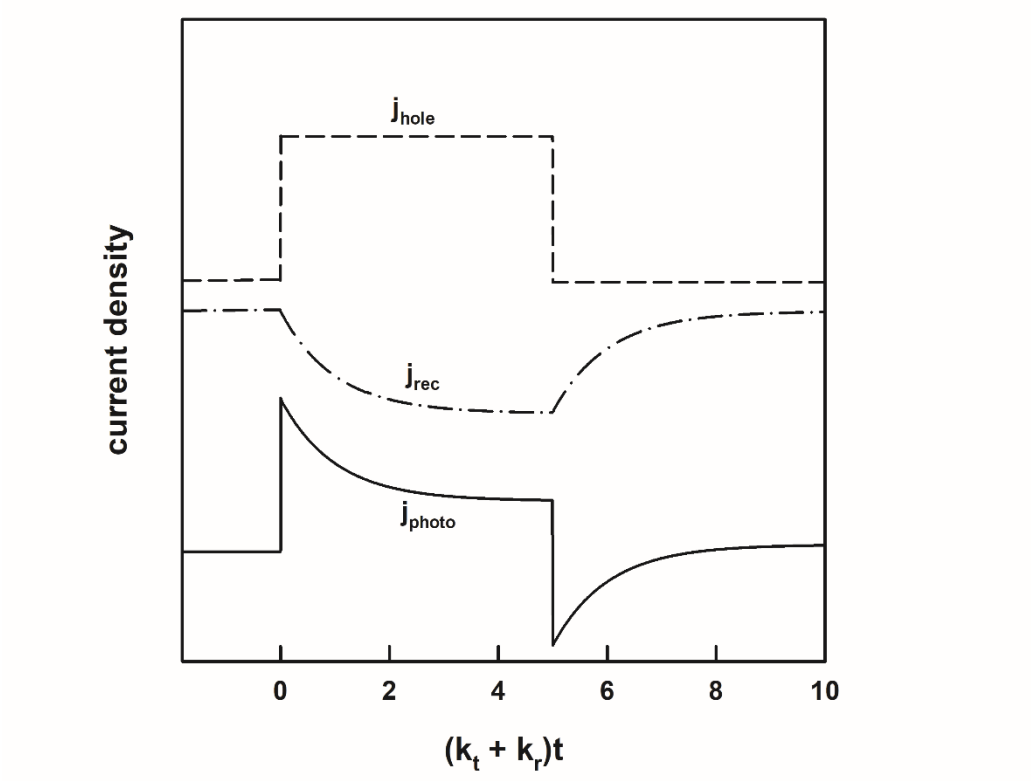

Figure 5. Normalized photocurrent transient predicted (j_{photo}) for the case where no band edge unpinning occurs. In this example η_{trans} = 0.3, i. $k_t/(k_t + k_r)$ = 0.3, so that the steady-state photocurrent is 30% of the initial value. Note the identical magnitudes of the decay and overshoot of the photocurrent. Compare this behaviour with Figure 1, where the negative overshoot is considerably smaller than the decay. The upper two plots show the positive hole current and the negative recombination current. The sum of these two currents determines j_{photo}. The plots have been offset on the vertical scale for clarity.

Figure 6 illustrates the deconvolution of the photocurrent transient into the charge transfer current and the charging current. Note that the initial current (t = 0) is entirely due to charging of the space charge capacitance, whereas at longer times approaching the steady state (before the light is switched off), the current is determined almost entirely by charge transfer. When the light is switched off, charge transfer continues, giving a positive current, but at the same time the double layer capacitance is discharged as holes are consumed, giving rise to a negative charging current that decays to zero.

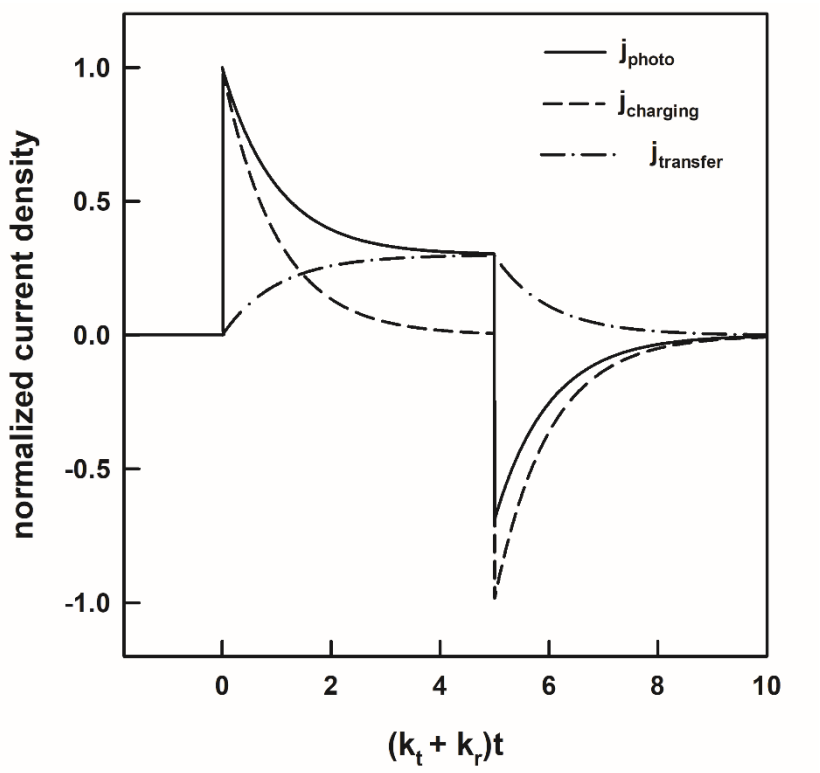

Figure 6. Deconvolution of the photocurrent into contributions from charge transfer and charging/discharging of the space charge capacitance. Calculation for $\eta_{ct} = k_t/(k_t + k_r) = 0.3$. The current scale is normalized to the hole current density qJ_G and the time scale to the decay time constant $(k_t + k_r)^{-1}$.

These simple analytical solutions are valid provided that the build-up of minority carriers is sufficiently small that we can neglect changes in the potential distribution across the interface brought about by the charging and discharging of the space charge capacitance. For this reason, IMPS measurements are normally carried out using a steady dc illumination level and a much smaller (a few%) superimposed sinusoidal modulation. Strictly speaking, even in this case it is necessary to consider the light-induced ac modulation of the band bending,[22] although this

is often neglected. The situation with large amplitude on-off illumination is different. If charge transfer is slow, the perturbation will change the surface concentration of minority carriers from a very low value in the dark to a much larger value under illumination. The minority carriers may be free (e.g. as holes in the valence band) or they may become trapped at surface states or as oxidized surface atoms (e.g. as Fe^{IV} states on hematite[10] – see below). The build-up of (in our case positive) charge in the photoelectrode will change the potential drops across the Helmholtz and space charge layers. The initial (dark) potential distribution is determined by the series connection of the space charge and Helmholtz capacitances.

$$\Delta\phi_{scr} = \left(E - E_{fb}\right)\frac{C_H}{C_{SCR}+C_H} \quad 8a)$$

$$\Delta\phi_H = \left(E - E_{fb}\right)\frac{C_{scr}}{C_{SCR}+C_H} \quad 8b)$$

where the space charge capacitance is given by the Mott Schottky equation.

$$\frac{1}{C_{SCR}^2} = \frac{2}{\varepsilon_r\varepsilon_{0q}N_d}\left(\Delta\phi_{scr} - \frac{k_BT}{q}\right) \quad 8c)$$

Under illumination, the potential distribution changes due to the build-up of holes at the interface by an amount

$$\delta\Delta V_H = -\delta\Delta\phi_{scr} = \frac{qp_{surf}}{C_H} \quad 8d)$$

We note in passing that one of the advantages of using a rough or nanostructured electrode is that the Helmholtz capacitance is increased and the surface hole concentration per unit area is decreased, both of which will reduce the extent of band edge unpinning under illumination (here we have assumed a reasonably flat surface).

Since the reduction in the band bending implied by equation 8 affects J_G, k_t and k_r, these three variables become functions of p_{surf}, and equation 3 takes the *non-linear* form

$$\frac{dp_{surf}}{dt} = J_{G,p_{surf}} - k_{t,p_{surf}}p_{surf} - k_{r,psurf}p_{surf} \quad 9)$$

To simplify the analysis, we have assumed that the rate of water oxidation is first order in hole concentration[25]. In the subsequent equations we omit the p_{surf} subscript for simplicity.

We now consider the way in which J_G, and k_r depend on $\delta\Delta\phi_{scr}$ as well as the dependence of k_t on $\delta\Delta V_H$. Equation 1 shows that the flux of holes J_G depends on the width of the space charge region, which in turn depends on $\Delta\phi_{scr}$ via equation 2. At the same time, we expect the pseudo-first order recombination rate constant k_r to depend on the concentration of electrons (majority carriers) at the surface (these electrons can be either in the conduction band or in surface states). If recombination occurs via surface states, recombination can be formulated using the Shockley Read Hall (SRH) approach.[27,28] As we have pointed out previously,[1] this leads to a non-linear expression for the time dependence of the recombination rate that would need to be solved numerically for large amplitude perturbations. Here we take a simpler approach by assuming the rate of surface recombination depends on the concentration of electrons at the surface in a way that can be expressed empirically as

$$k_r = k_{r,0} exp - \left(\frac{q\beta\Delta\phi_{scr}}{k_B T}\right) \quad 10)$$

Here $k_{r,0}$ corresponds to the first order recombination rate constant for zero band bending. One of the puzzling features of surface recombination at hematite electrodes is that it is so slow. The value measured of k_r measured by IMPS for a dc photon flux equivalent to one sun is only 10^2 s^{-1} at an estimated band bending of 0.4 – 0.5 eV, and the rather weak potential dependence of k_r corresponds to a value of β = 0.12[14] (the weak potential dependence of k_r may be the consequence of non-ideal behaviour arising from the storage of charge in surface states). Based on equation 10, $k_{r,0}$ for hematite would be ca. 10^3 s^{-1}. This very low value strongly suggests that 'recombination' may in fact be an activated process involving chemical change at the surface rather than the annihilation of holes by electrons. This point is discussed further in section 4.

This leaves the dependence of k_t on ΔV_H, which is rarely considered. One of the few papers to discuss this issue is by Waegele et al.[29] who used intense laser pulses to induce band edge unpinning in n-$SrTiO_3$ photoanodes. These authors reported a Tafel-like dependence

of the rate constant on ΔV_H for the first (very fast) hole transfer in water oxidation. Our own work has shown that k_t measured for untreated hematite electrodes increases in a quite complex way with bias potential.[14] To simplify the modelling, we adopt the normal approach used for metal electrodes and formulate the dependence of k_t on ΔV_H using the Tafel expression.

$$k_t = k_{t,0}\exp\left(\frac{\gamma q \delta \Delta V_H}{k_B T}\right) \qquad 11)$$

Here γ replaces the more familiar α, the transfer coefficient (in this case, the anodic transfer coefficient). Waegele et al. reported values of the transfer coefficient in the range 0.2 – 0.25 for the first step of water oxidation on $SrTiO_3$, which they propose leads to a surface-bound hydroxyl radical species.

We now have expressions that specify all three the non-linear terms in equation 8, so numerical solutions of the photocurrent transient problem become possible. A link to the numerical solution in Matlab is given in Appendix C.

3. Results of the Modelling

We begin by choosing materials parameter values that are reasonable for hematite photoanodes illuminated at 455 nm, namely ε_r = 25, $N_d = 10^{19}$ cm^{-3}, $\alpha = 10^5$ cm^{-1}, L_p = 1 nm. In addition, we take $\beta = \gamma = 0.20$, $k_{t,0} = 1$ s^{-1}, $k_{r,0} = 10^2$ s^{-1} and C_H = 100 μF cm^{-2} to allow for some surface roughness. Calculations of the transient response were performed for an incident photon flux $I_0 = 10^{16}$ cm^{-2} s^{-1}.

Figure 7 contrasts the transient photocurrent response in the absence of band edge unpinning with the response calculated numerically for the parameter values shown.

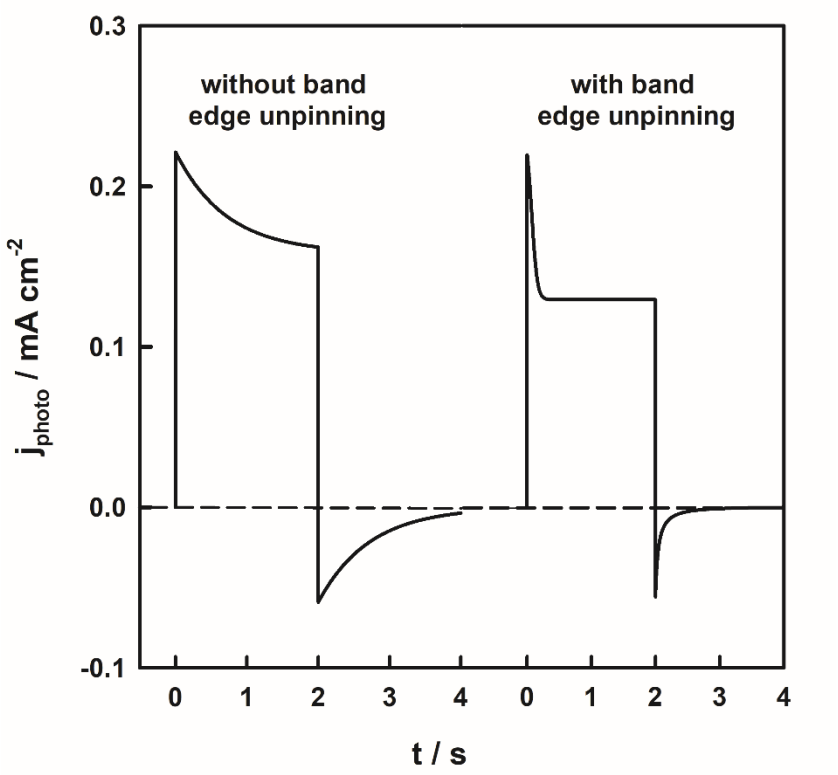

Figure 7. Photocurrent transients calculated with and without band edge unpinning for an incident photon flux I_0 = 10^{16} cm^{-2} s^{-1}, $E - E_{fb}$ = 0.7V. Other parameters: $k_{t,0}$ = 1 s^{-1}, $k_{r,0}$ = 10^2 s^{-1}, $\beta = \gamma$ = 0.2, ε = 25, N_d = 10^{19} cm^{-3}, α = 10^5 cm^{-1}, L_p = 1 nm, C_H = 100 μF cm^{-2}. In the right hand transient, note the difference in magnitude between the decay $j_{photo}(t = 0)$ - $j_{photo}(t \rightarrow \infty)$ and the negative overshoot. The additional suppression of the 'on' photocurrent arises from band edge unpinning and the resulting reduction in the potential drop across the space charge region, which accelerates both recombination and charge transfer.

The consequences of bend edge unpinning for the symmetry of the on and off transients is now evident in the photocurrent response. The much faster decay in the right-hand transient is primarily caused by band edge unpinning, which in this case reduces the potential drop across the space charge region from 0.68 V to 0.46 V, as shown below.

The substantial band edge unpinning that arising from the build-up of holes at the interface is evident from the time-dependent behaviour of $\Delta\phi_{scr}$ shown in Figure 8.

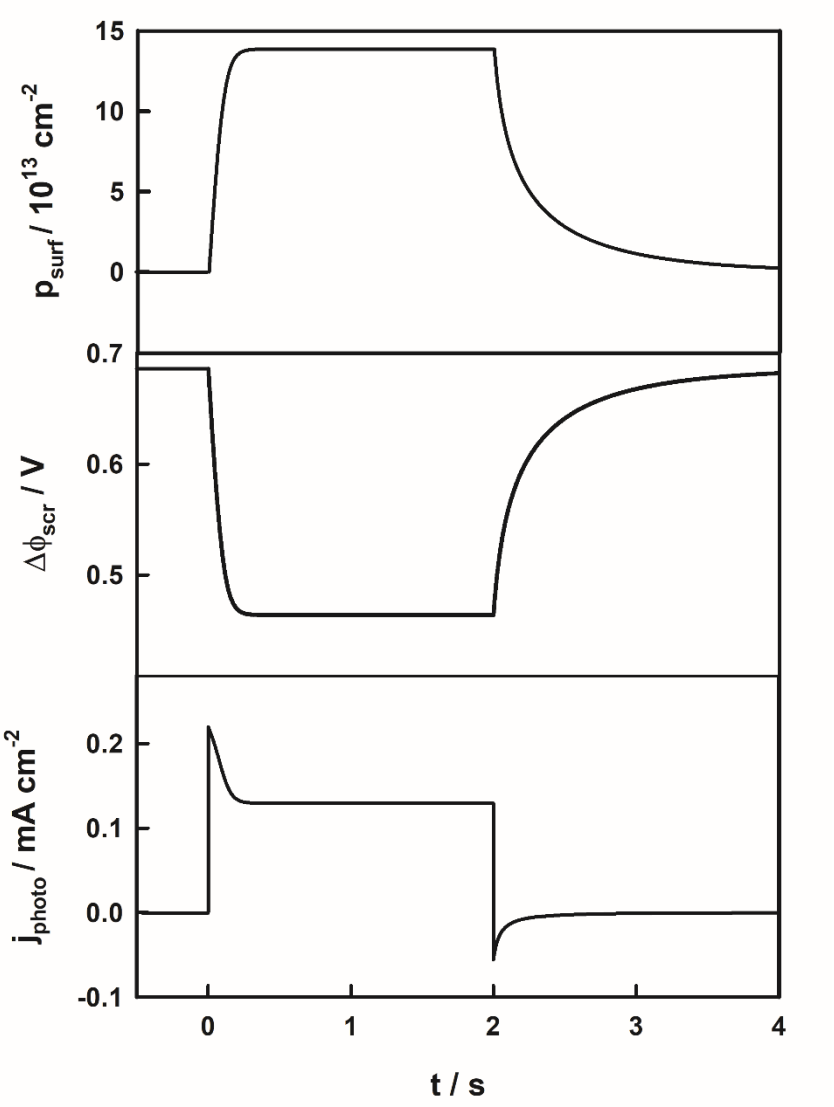

Figure 8. Build-up and decay of surface hole concentration and corresponding reduction in the potential drop across the space charge region occurring during the photocurrent transient (cf. Figure 7). Contrast the asymmetric on/off plot of the surface hole concentration with the symmetrical plot in the absence of band edge unpinning shown in Figure 4. This strong asymmetry in the hole concentration plots has been seen in optical absorbance measurements on for hematite photoanodes[25] and in microwave reflectance measurements on p-type silicon photocathodes[7].

The most obvious difference between Figures 5 and 8 is that the symmetry in the build-up and decay of the hole concentration is lost when band edge unpinning occurs. The build-up of hole concentration is much faster than the subsequent decay in the dark. This result is significant because this behaviour has been reported in the literature. An excellent example is the work of Le Formal et al.[25] who used photoinduced absorbance (PIA) to follow the surface hole concentration during water oxidation on hematite electrodes on a long timescale (the 'on' time in these experiments was 5 seconds). At lower light intensities (ca. 10^{14} cm^{-2} s^{-1}

at 365 nm), the rise and decay of the PIA signal are symmetrical but increasing the light intensity in steps up to a maximum of ca. 10^{17} cm^{-2} s^{-1} leads to a much more rapid rise of the absorbance, while the decay remains largely unaffected. The PIA transients for high intensities shown in Figure 2 of the Le Formal paper closely resemble those in Figure 7, albeit on a somewhat longer timescale. Similarly, microwave measurements of the excess electron concentration in p-Si photocathodes by Cass et[7] al. show exactly the same kind of asymmetric response as shown in Figure 8, and in this case band edge unpinning was confirmed by transient capacitance measurements (cf. Figures 5 and 10 of the paper by Cass et al.).

Inspection of equations 10 and 11 shows that band edge unpinning that results from the build-up of holes at the surface increases both k_r and k_t. Figure 9 illustrates this effect for the photocurrent transient in Figure 7.

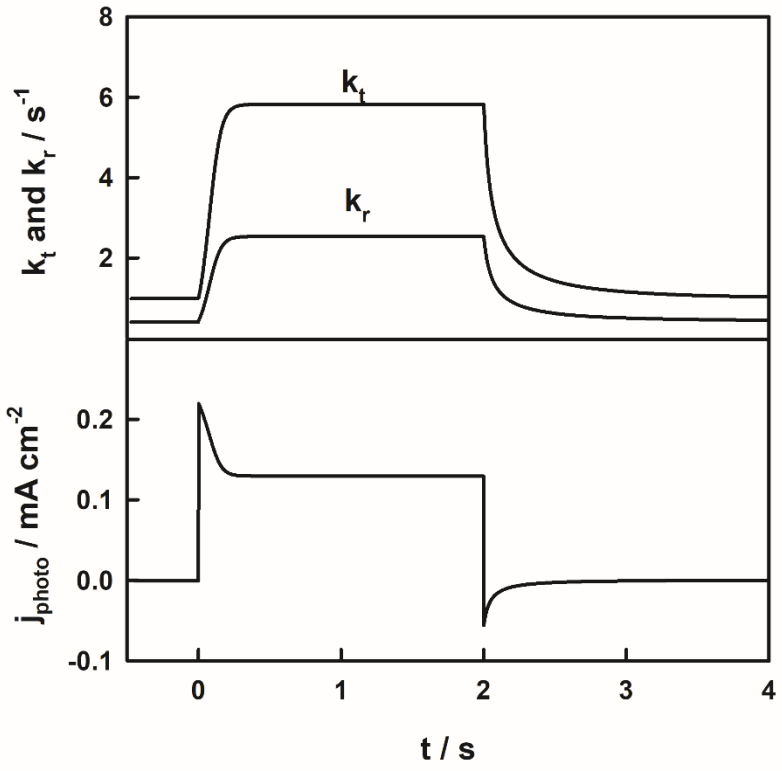

Figure 9. Effect of band edge unpinning on the rate constants for charge transfer (k_t) and recombination (k_r) during the photocurrent transient. The rate constant for recombination increases due to the lowering of the band bending under illumination, and the charge transfer rate constant also increases due to the increase in the potential drop across the Helmholtz layer. Since in this calculation, $\beta = \gamma = 0.2$, the change in potential distribution increases both k_r and k_t by the same factor and the charge transfer efficiency therefore remains constant ($\eta_{trans} = 0.7$).

The reduction in the width of the space charge region caused by band edge unpinning under illumination decreases the flux of holes to the surface as shown in Figure 10. This leads to a further reduction of the steady state photocurrent.

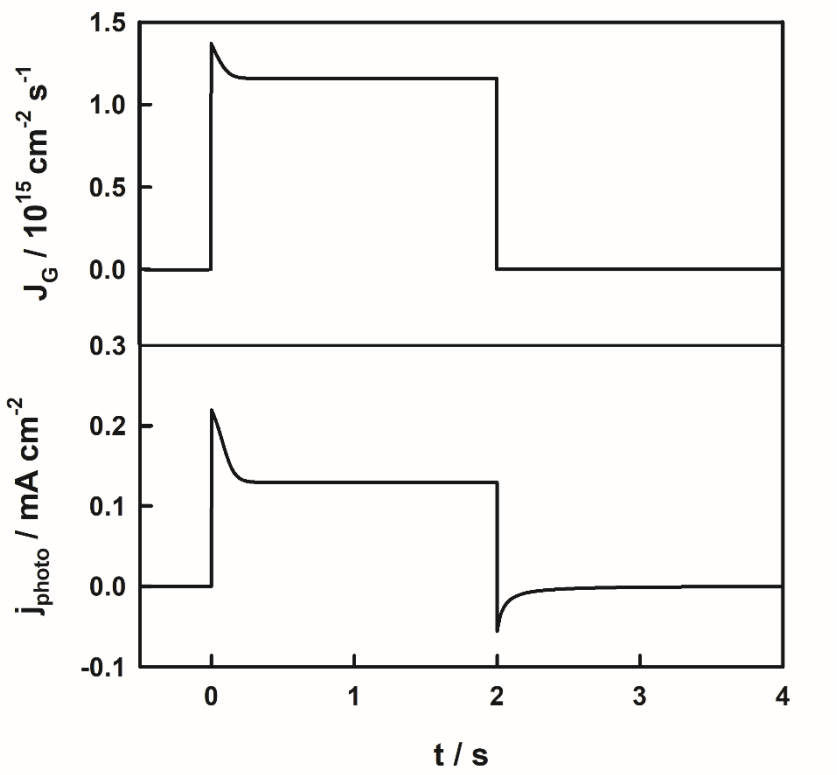

Figure 10. Reduction in the J_G, the flux of holes, during the photocurrent transient as the result of band edge unpinning and the consequent reduction of the width of the space charge region.

As mentioned above, band edge unpinning can be detected using transient capacitance measurements.[7, 30] Figure 11 shows the calculated transient change in the space charge capacitance associated with the photocurrent transient.

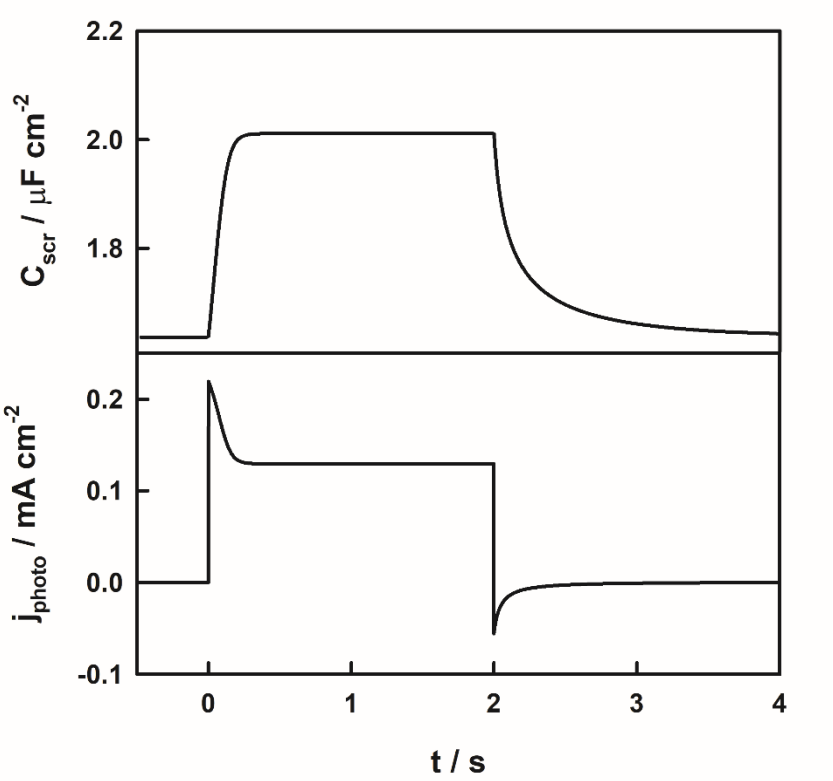

Figure 11. Transient change in space charge capacitance during the photocurrent transient.

Finally, when the applied voltage is increased sufficiently, recombination becomes unimportant so that band edge unpinning is entirely responsible for the decay of the photocurrent and the overshoot disappears, as shown in Figure 12 for an applied voltage (E – E_{fb} (dark) = 1.2 V (other variables are the same as for Figure 7).

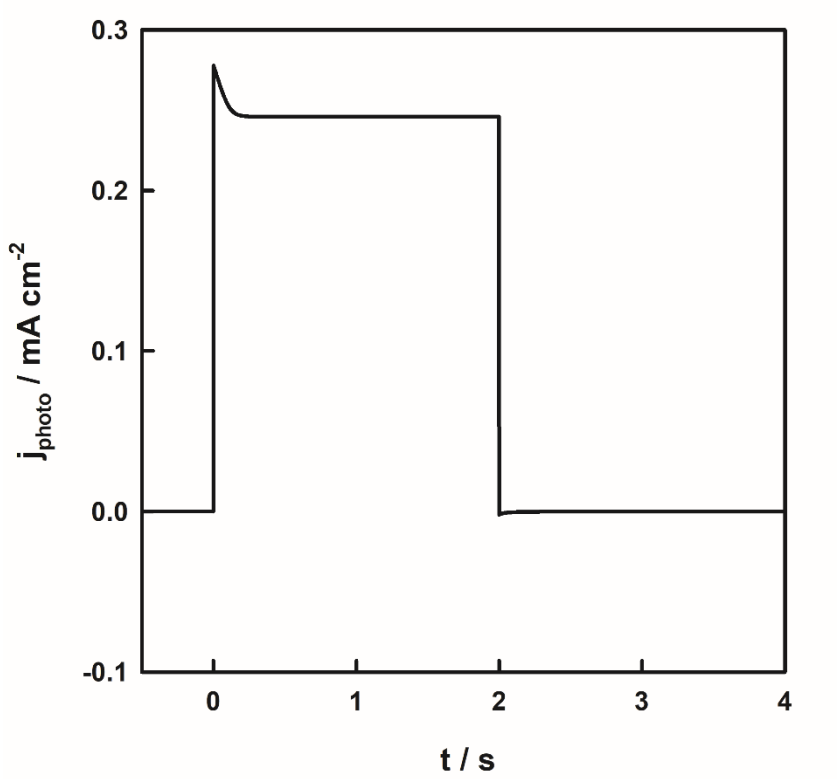

Figure 12. Calculated photocurrent transient showing absence of overshoot at a higher applied voltage ($E - E_{fb}$ = 1.2 V). In this case, the decay of the photocurrent is entirely due to the reduction in the width of the space charge region – and hence of J_G - arising from band edge unpinning (see Figure 10). Other parameter values as for Figure 7.

An interesting consequence of the dependence of k_t on ΔV_H is that at higher potentials, where recombination is negligible, the surface hole concentration does not increase linearly with intensity, whereas the photocurrent does. The reason is simple: the build-up of holes increases ΔV_H, thereby increasing the rate constant for hole transfer. For the set of variable values used here, the calculation predicts that k_t will increase by around a factor 50 when the intensity is increased from 10^{13} cm^{-2} s^{-1} to 10^{17} cm^{-2} s^{-1}.

Figure 13 shows the non-linear behaviour of the surface hole concentration predicted for $E - E_{fb}$ = 1.5 V for the same variable values used in the preceding calculations. The plot matches rather well the experimental result measured by Le Formal et al. [25] for a hematite electrode using photoinduced absorbance. The plot of steady-state photocurrent is only slightly sub-linear (the deviation at $I_0 = 10^{17}$ cm^{-2} s^{-1} is only -15%), whereas the plot of p_{surf} is highly

non-linear because k_t increases exponentially with the potential drop across the Helmholtz layer cf. equation 11).

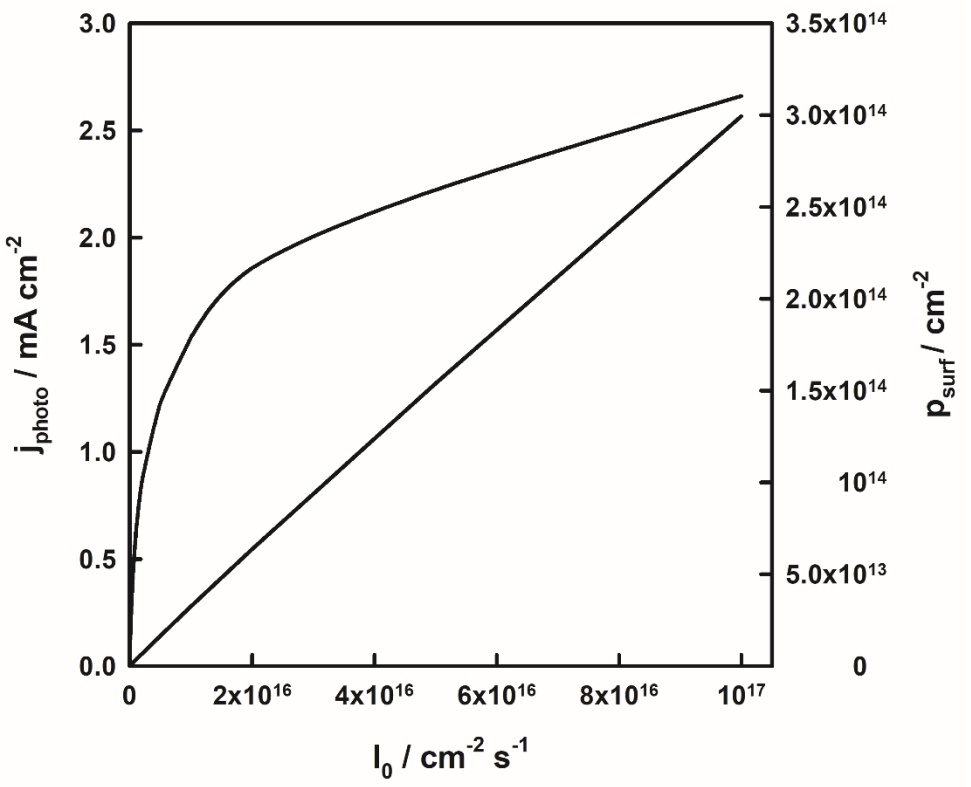

Figure 13. Light intensity dependence of the steady-state photocurrent and steady state surface hole concentration calculated for $E - E_{fb}$ = 1.5 V. Other variable values are the same as for Figure 7. The non-linearity of the hole concentration plot arises from the exponential increase in k_t as the voltage drop ΔV_H increases with increasing build-up of holes at the interface. By contrast, the photocurrent is an almost linear function of light intensity (the sub-linear deviation at the highest intensity is only 15%).

The non-linear dependence of p_{surf} on photocurrent has been interpreted by Le Formal et al in terms of the reaction order with respect to hole concentration of the overall oxygen evolution reaction. Based on a log-log plot of photocurrent vs. hole concentration, these authors concluded that the reaction order varies from 1 at low intensities to 3 at high intensities. In order to see if this behaviour could be explained by band edge unpinning and the resulting increase in the first order rate constant k_t, the data in Figure 13 have been replotted as a log-log plot as shown in Figure 14. The plot shows that the reaction order with respect to p_{surf} does indeed appear to change from 1 to 3 as the intensity is increased. However, in our calculations, the reaction order is 1, and the change in slope is due to the 50-fold increase in k_t resulting from the increased driving force for hole transfer associated with band edge unpinning (cf. equation

10 which represents the exponential Tafel dependence of k_t on ΔV_H). The increase in ΔV_H and k_t with light intensity is illustrated in Figure 15 for the same set of variables as those used to calculate Figure 13.

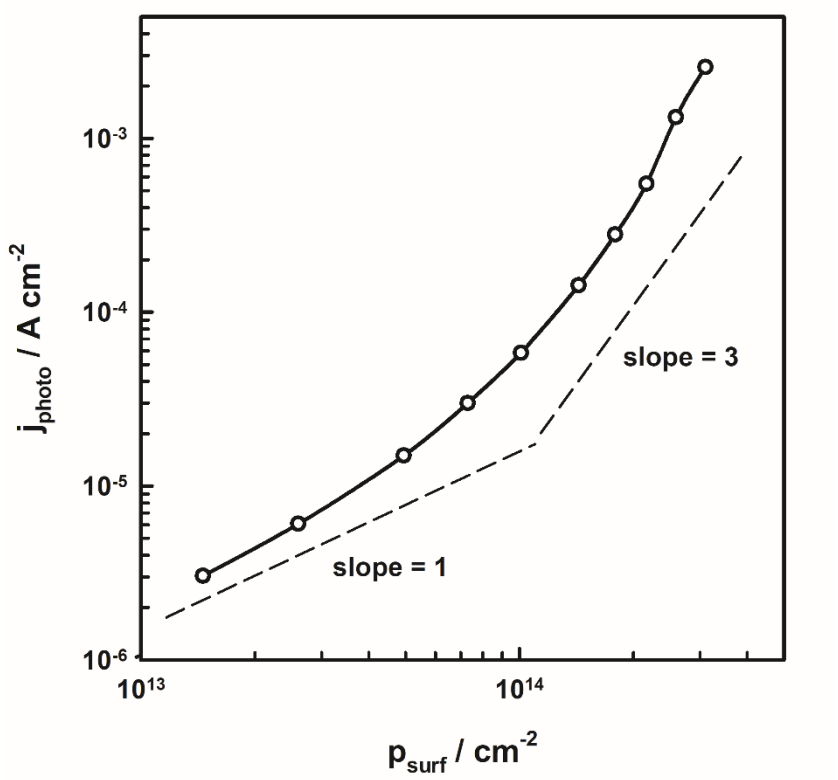

Figure 14. Double logarithmic 'reaction order' plot of j_{photo} vs. p_{surf} constructed from the data in Figure 13. The slope of the plot corresponds to the apparent reaction order of the reaction on the surface hole concentration. In fact, the change in slope of the plot is due to the increase in the rate constant for hole transfer associated with band edge unpinning (i.e. increase in potential drop across the Helmholtz layer: cf. equation 11). The dashed lines show the slopes for nominal reaction orders of 1 and 3 with respect to hole concentration.

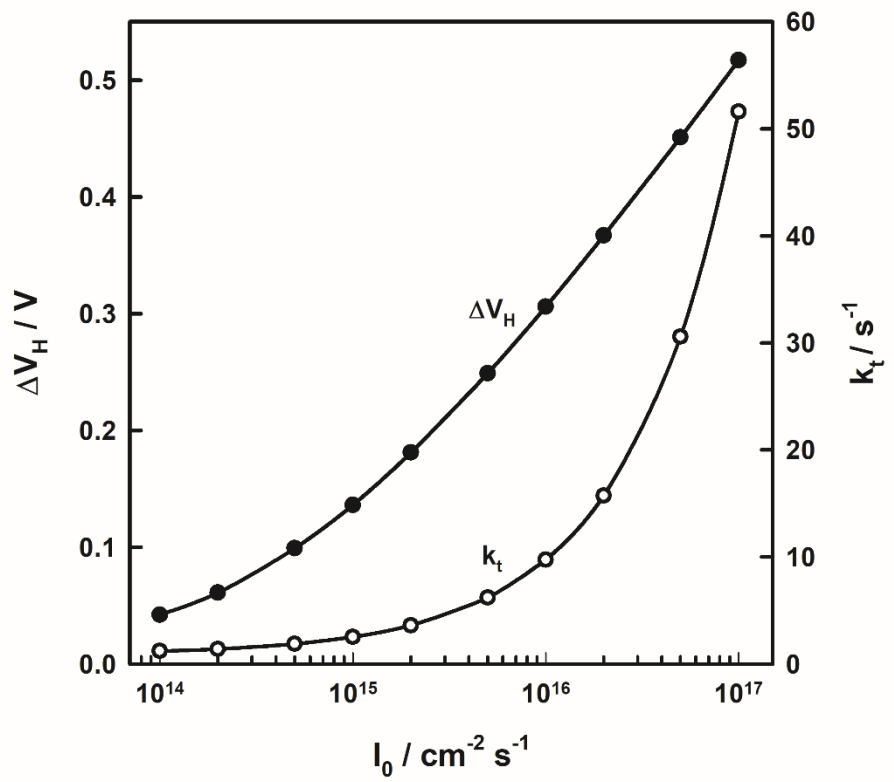

Figure 15. Intensity-dependent changes in ΔV_H, the potential drop in the Helmholtz layer and k_t, the rate constant for hole transfer that explain the plots in Figures 11 and 12. $E - E_{fb}$ = 1.5 V. Other parameters as in Figure 7. Note the fifty-fold increase in k_t predicted by equation 11 (with γ = 0.20) that explains why the surface hole concentration does not increase linearly with intensity.

4. Discussion of experimental transients: limitations of the model

The results of the modelling show that care is needed when interpreting on-off photocurrent transients produced by high intensity illumination because the build-up of charges at the surface can cause band edge unpinning, which alters the potential distribution across the semiconductor/electrolyte interface and hence the rate constants for recombination and charge transfer. The question now arises, can the modelling explain the results in Figures 1 to 3?

Figure 1 showed the transient response of an annealed hematite layer prepared by AACVD using ferrocene as precursor. In this case, it appears that the asymmetric transient photocurrent response can be explained in terms of band edge unpinning. However, quantitative comparison is complicated by the fact that the hematite layer is nanostructured on the scale of a few hundred nanometres. Provided that the width of the space charge region is smaller than the crystallite size, the basic concepts of the model are still applicable, although the hole flux is now lower

because it takes place into the internal surface area of the porous layer. At the same time, the Helmholtz capacitance is increased by the surface roughness factor, which for similar films is reported to be around 20.[25] The surface roughness will therefore reduce the effects of band-edge unpinning. In fact, the experimental transient was measured for an incident photon flux ten times higher (10^{17} cm^{-2} s^{-1}) than the value used in the calculations, so that the band edge unpinning in both cases should be similar taking the surface roughness into account.

By contrast, several aspects of the transients in Figures 2 and 3 are puzzling. Why is the rise time of the photocurrent in the case of the ultrathin ALD hematite layer so slow, whereas the negative current overshoot is much faster? Why do the transients for p-type lithium doped CuO in Figure 3 become smaller with successive light pulses? At this point it is appropriate to widen the discussion to consider other effects that can influence the shape of photocurrent transients.

The theory that is outlined in section 2 is based in the assumption that the photoelectrode is both macroscopic and reasonably planar so that both the illumination and the charge separation by drift diffusion take place in a direction that is normal to the electrode surface. If the electrode is nanostructured, different approaches to the minority carrier generation/collection problem are necessary, as we have discussed elsewhere.[24] As pointed out in section 3, provided that the material is sufficiently highly doped that the space charge region is smaller than the characteristic feature size (e.g. nanowire radius), a similar approach involving the superimposition of displacement and recombination currents is still possible, and this appears to be the case for the hematite sample prepared by AACVD. However, in the case of mesoporous layers of lower doped materials in which the band bending is severely limited by the size of the particles,[31] carrier transport is likely to be controlled by trap-limited diffusion. For such cases, a different approach will be necessary.

So far, we have not discussed where exactly the minority carrier charge is located or what 'chemical' nature it might have. As far as the electrostatic effect of the excess minority carrier charge is concerned, we have simply used the total free excess hole charge to calculate the change in the potential distribution across the junction. However, in the case of hematite, we know from in-situ spectroscopic studies that illumination generates what appear to be Fe(IV) species at the surface.[10] These species are probably identical with the 'long-lived holes' observed by transient absorption spectroscopy.[32] This raises questions about the location and chemical identity of the 'hole'. If holes are indeed 'trapped' by chemical reaction with surface Fe(III) sites, we may envisage that the reaction is

$$\text{Fe-OH} + h^+ \rightarrow \text{Fe=O} + H^+ \qquad 12)$$

(in alkaline solution, the proton will form H_2O). The hole has now disappeared and instead a new surface group has been created with a different surface dipole, changing the work function of the semiconductor. The positive charge has been transferred to the solution so that it can no longer give rise to a change in the potential drop across the Helmholtz layer. 'Recombination' would then be due to electron capture by the Fe(IV) species to reform Fe(III). Further intermediate states in the 4-electron 4-proton oxygen evolution reaction could also modify the potential distribution in the same way as well as take part in 'recombination'. The calculation of the change in potential distribution across the interface would require knowledge of the dipole moments of the initial and final bonded states. Nevertheless, formulation of the kinetics to predict transients is still possible in principle – instead of building up holes at the surface, we could consider the increase in the surface concentration of Fe(IV) species and the resulting change in surface dipole. The modelling would require equation 8d to be replaced by an expression related to the change in surface dipole, but such an approach lies outside the scope of this paper.

The situation with hydrogen evolution on p-type materials can be equally complex. For example, in the case of hydrogen evolution on p-GaAs, Erné et al. have used in situ infrared spectroscopy to show that the reaction involves changing the surface termination from As-OH via unterminated As· to As-H.[33] In this case, the anodic photocurrent overshoot arises from oxidation of surface-bound hydrogen by holes rather than from electron-hole recombination. By analogy, in the case of hematite photoanodes, the cathodic overshoot may well correspond to reduction of surface Fe=O species by electrons to form Fe-OH rather than electron-hole recombination in the conventional sense. This interpretation would certainly be consistent with spectroelectrochemical[10] and transient absorption[25] measurements.

We also need to remember that the potential drop across the photoelectrode/electrolyte interface is determined not only by the electronic charge and by the surface dipoles associated with the termination of the semiconductor lattice by chemical groups bonded to the surface but also by oriented solvent molecules as well as by the ionic surface charge associated with the acid/base properties of the semiconductor itself or of surface oxides. The latter effect introduces a pH-dependent ionic surface charge and hence potential drop. In the modelling in the previous section, we have assumed that all these contributions to the potential drop remain unchanged under illumination. In the case of water splitting reactions, we know that the intermediates in the multistep electron/proton transfer reaction must be bound to the electrode surface. Furthermore, the photoelectrolysis reactions will lead to changes in local pH: in the case of oxide photoanodes, for example, the decrease in pH due to oxygen evolution will shift the flatband potential to more positive values, decreasing the band bending for a fixed applied voltage. Similarly, the increase in pH associated with hydrogen evolution at p-type cathodes will shift the flatband potential to more negative values, again decreasing the band bending for a fixed applied voltage. The effects of pH changes will be most evident in the case of unbuffered electrolyte solutions and high photocurrents. In view of the complications identified

in the preceding discussion, we conclude that our model represents a simplification and generalization that should be used with care.

Returning to the experimental results, it will be clear by now that the model does not explain the slow rise of the photocurrent measured in the case of thin ALD layers of hematite. A finite rise time is expected, of course, as a result of the RC time constant of the series resistance and electrode capacitance, but this RC pulse shaping should affect both the on and off transient, which is clearly not the case here. It therefore appears that there is a delay in holes reaching the surface. Our model has assumed rapid displacement of free photogenerated charges in the space charge region, but if charge trapping occurs, carriers will reach the surface by a sequence of trapping and detrapping events. Slow photocurrent risetimes are characteristic of systems with multiple trapping: the best-known example is the dye-sensitized solar cell.[34] We therefore tentatively attribute the slow risetime of the anodic photocurrent to hole trapping [35] or polaron formation[36]in the ALD hematite layer. The fast negative 'off' transient suggests that the electron mobility in the ALD layers is much less affected by trapping or polaron formation.

The photocathodic transients for lithium-doped CuO could in principle be due to band edge unpinning by the build-up of electrons at the interface, but one could also envisage formation of surface Cu(I) species resulting from electron capture by Cu(II) states. Recombination would then correspond to oxidation by holes of Cu(I) back to Cu(II). This raises the question whether the photocurrent is indeed due to hydrogen evolution rather than photocathodic reduction of CuO to Cu_2O or to Cu. To investigate this, a hydrogen sensor was used to confirm that the Faradaic efficiency for hydrogen production is close to 100%. The fact that the photocurrent spikes become smaller on successive light pulses led us to suspect that the increase in pH associated with hydrogen evolution shifts the flatband potential to progressively more negative values, thereby decreasing the band bending in the photocathode and hence the photocurrent.

The ca. 1 mA cm^{-2} photocurrent pulses will each generate around 50 nanomoles cm^{-2} of OH^-. To obtain an idea of the local OH^- concentration, we consider that the photoelectrochemical reaction in an unstirred solution will create a diffusion layer in solution with an order of magnitude thickness of $(D_{OH^-}t)^{1/2} \approx 200$ μm. At the end of the light pulse, the surface concentration of OH^- will be of the order of several mM, so that since the solution is unbuffered, the pH will have increased by 3 pH units during the light pulse, which corresponds to a negative shift of the flatband potential by around 180 mV, enough to cause the decay seen in the photocurrent.

5. Conclusions

An important conclusion is that the interpretation of both steady state and transient kinetic measurements of photoelectrode processes need to take band edge unpinning into account. The quantitative model developed in this paper suggests different ways of detecting band edge unpinning. Direct optical or microwave measurement of the hole concentration should allow comparison with the calculated p_{surf} transients. Strong asymmetry (fast rise and slow decay) indicates that band edge unpinning is occurring. Similarly, measurement of the transient photocapacitance provides an indirect measurement of the changes in band bending. Again, strong asymmetry in the on and off photocapacitance responses would indicate that band edge unpinning is occurring.

More sophisticated 3-D optical and electrochemical modelling for nanostructured electrodes used for photoelectrochemical water splitting should be possible using the basic concepts outlined here. However, progress in understanding at the molecular level will also depend on the extent to which non-electrochemical techniques can help to unravel the kinetics and mechanism of the reactions taking place. We hope that the present paper offers a suitable starting point for further quantitative theoretical and experimental studies of the kinetics and mechanisms of light-driven water splitting.

Acknowledgments

ABW acknowledges funding from the European Union's Horizon 2020 Research and Innovation Programme under the EoCoE II project (824158).

Appendix A. List of Symbols

$\alpha(\lambda)$: absorption coefficient at wavelength λ.

β: empirical factor for dependence of recombination rate constant on band bending.

$\Delta\phi_{scr}$: potential drop across the space charge region.

γ: transfer coefficient in Tafel equation for electron transfer rate constant.

ΔV_H: change in voltage drop across Helmholtz layer caused by carrier build-up.

ε_r: relative permittivity of semiconductor.

ε_0: permittivity of free space.

η_{ct}: charge transfer efficiency.

τ: light on period.

C_H: Helmholtz capacitance.

C_{scr}: space charge capacitance.

E: applied potential vs. a reference electrode

E_{fb}: flat band potential vs. the same reference electrode.

I_0: incident photon flux corrected for reflection loss.

J_G: minority carrier flux into the surface predicted by the Gärtner equation.

$J_{G,psurf}$: minority carrier flux in presence of band edge unpinning (depends on p_{surf}).

j_{photo}: photocurrent density.

k_B: Boltzmann constant.

k_r: first order surface recombination constant.

$k_{r,0}$: recombination rate constant for zero band bending.

$k_{r,psurf}$: recombination rate constant in presence of band edge unpinning (depends on p_{surf}).

k_t: first order rate constant for transfer of minority carriers to solution species.

$k_{t,0}$: rate constant for transfer in the absence of band edge unpinning.

$k_{t,psurf}$: rate constant for charge transfer in presence of band edge unpinning(depends on p_{surf}).

L_p: hole diffusion length.

N_d: donor density.

$n_{x=0}$: electron density (per unit volume|) at photoelectrode surface.

p_{surf}: surface hole density (per unit area).

q: elementary charge.

W_{scr}: width of the space charge region.

Appendix B. Sample Preparation

The preparation of the ALD hematite photoanodes has been previously reported.[37] Briefly, the FTO substrates were precleaned by successive sonication with detergent, DI water and isopropanol dried and placed in a Picosun R-200 Advanced ALD reactor at 250°C. They were then subjected to 450 ALD cycles. Each cycle consisted of a 1.5 s dosing of ferrocene gas (Aldrich, 98%, sublimed from a stainless-steel container at 90°C), 7 s exposure and 8 s nitrogen purge followed by a 6 s dosing of ozone, 7 s exposure and 8 s purge. The purge gas was 99.999 % nitrogen and the base pressure between dosings was approximately 6 hPa. The processed samples were placed in a muffle furnace, heated to 600°C in air over 3 h and held at that temperature for 30 min. After cooling the active area was masked using PTFE adhesive tape and the FTO substrate was contacted using conductive silver paste.

LixCu1-xO photocathode layers were prepared by spin coating an ethanolic solution of $Cu(NO_3)_2{\cdot}3\ H_2O$ and $LiNO_3$ onto FTO substrates. Calcination of these coatings at 400 °C resulted in homogeneous black films. Unreacted $LiNO_3$ and $LiCO_3$ were removed by rinsing in water. XRD analysis revealed that the Li-doped phase is structurally closely related to CuO tenorite (space group: *C2/c)* but with slightly different unit cell parameters (a = 4.6850(1) Å, b = 3.4263(1) Å, c = 5.1318(1) Å and β = 99.445(1)°) as compared to pure CuO phase (a = 4.6853(3) Å; b = 3.4257(1) Å; c = 5.1303(3) Å; β = 99.549(4)°). The resulting in the small increase of the unit cell volume from 81.20(1) $Å^3$ in the pure CuO to 81.26(1) $Å^3$ in the Li-doped CuO is consistent with incorporation of a small amount of lithium ions, which have a slightly larger ionic radius (0.76 Å) than Cu^{2+} ion (0.73 Å). ICP-AAS analysis showed that that Li ions content in the films was 1.3 at-%. During the photocurrent measurements a calibrated hydrogen needle sensor (Unisense, H2-NPLR) was used to monitor the change in hydrogen concentration over time.

Appendix C. Numerical Solution

The model has been coded in Matlab. The programs and notes are available on Mendeley data:

here: DOI to be added at proof stage.

References

[1] L.M. Peter, J. Li, R. Peat, Surface recombination at semiconductor electrodes. Part I. Transient and steady-state photocurrents, J. Electroanal. Chem. Interfacial Electrochem. 165(1-2) (1984) 29-40.

[2] J. Li, L.M. Peter, Surface recombination at semiconductor electrodes. Part III. Steady-state and intensity modulated photocurrent response, J. Electroanal. Chem. Interfacial Electrochem. 193(1-2) (1985) 27-47.

[3] J. Li, L.M. Peter, Surface recombination at semiconductor electrodes. Part IV. Steady-state and intensity modulated photocurrents at n-gallium arsenide electrodes, J. Electroanal. Chem. Interfacial Electrochem. 199(1) (1986) 1-26.

[4] J. Li, R. Peat, L.M. Peter, Surface recombination at semiconductor electrodes. Part II. Photoinduced "near-surface" recombination centers in p-gallium phosphide, J. Electroanal. Chem. Interfacial Electrochem. 165(1-2) (1984) 41-59.

[5] L.M. Peter, Dynamic Aspects of Semiconductor Photoelectrochemistry, Chem. Rev. 90(5) (1990) 753-769.

[6] M.J. Cass, N.W. Duffy, L.M. Peter, S.R. Pennock, S. Ushiroda, A.B. Walker, Microwave reflectance studies of photoelectrochemical kinetics at semiconductor electrodes. 1. Steady-state, transient, and periodic responses, J. Phys. Chem. B 107(24) (2003) 5857-5863.

[7] M.J. Cass, N.W. Duffy, L.M. Peter, S.R. Pennock, S. Ushiroda, A.B. Walker, Microwave reflectance studies of photoelectrochemical kinetics at semiconductor electrodes. 2. Hydrogen evolution at p-Si in ammonium fluoride solution, J. Phys. Chem. B 107(24) (2003) 5864-5870.

[8] S.R. Pendlebury, A.J. Cowan, M. Barroso, K. Sivula, J. Ye, M. Grätzel, D.R. Klug, J. Tang, J.R. Durrant, Correlating long-lived photogenerated hole populations with photocurrent densities in hematite water oxidation photoanodes, Energy & Environmental Science 5(4) (2012) 6304-6312.

[9] M. Barroso, S.R. Pendlebury, A.J. Cowan, J.R. Durrant, Charge carrier trapping, recombination and transfer in hematite (alpha-Fe_2O_3) water splitting photoanodes, Chemical Science 4(7) (2013) 2724-2734.

[10] C.Y. Cummings, F. Marken, L.M. Peter, K.G.U. Wijayantha, A.A. Tahir, New Insights into Water Splitting at Mesoporous alpha-Fe_2O_3 Films: A Study by Modulated Transmittance and Impedance Spectroscopies, J. Am. Chem. Soc. 134(2) (2012) 1228-1234.

[11] R. Haak, D. Tench, Electrochemical Photocapacitance Spectroscopy Method for Characterization of Deep Levels and Interface States in Semiconductor Materials, J. Electrochem. Soc. 131(2) (1984) 275-283.

[12] P. Allongue, H. Cachet, Photocapacitance study of n-GaAs/electrolyte interfaces, Berichte der Bunsengesellschaft für physikalische Chemie 91(4) (1987) 386-390.

[13] C.Y. Cummings, F. Marken, L.M. Peter, A.A. Tahir, K.G.U. Wijayantha, Kinetics and mechanism of light-driven oxygen evolution at thin film alpha-Fe_2O_3 electrodes, Chem. Commun. 48(14) (2012) 2027-2029.

[14] L.M. Peter, K.G.U. Wijayantha, A.A. Tahir, Kinetics of light-driven oxygen evolution at alpha-Fe_2O_3 electrodes, Faraday Discuss. 155 (2012).

[15] S. Saremi-Yarahmadi, A.A. Tahir, B. Vaidhyanathan, K.G.U. Wijayantha, Fabrication of nanostructured alpha-Fe_2O_3 electrodes using ferrocene for solar hydrogen generation, Mater. Lett. 63(5) (2009) 523-526.

[16] A.G. Hufnagel, Atomic Layer Deposition for Energy Conversion and Storage, PhD Thesis, Department of Chemistry and Center of Nanoscience, LMU Munich, Munich, 2018, p. 273.

[17] I.T. Kondofersky, Desigan of Photoeletrode Morphologies for Solar-Driven Water Splitting, Department of Chemistry and Center for Nanoscience, PhD Thesis, LMU Munich, Munich, 2016.

[18] C.-Y. Chiang, Y. Shin, S. Ehrman, Li Doped CuO Film Electrodes for Photoelectrochemical Cells, J. Electrochem. Soc. 159(2) (2011) B227-B231.

[19] L.M. Peter, D. Vanmaekelbergh, Time and frequency resolved studies of photoelectrochemical kinetics, in: R.C.K. Alkire, D.M. (Ed.), Adv. Electrochem. Sci. Eng., Weinheim, 1999, pp. 77-163.

[20] D. Meissner, C. Sinn, J. Rimmasch, R. Memming, B. Kastening, Pinning and Unpinning of Band Positions at the Semiconductor/Electrolyte I nterface, in: W.H. Bloss, F. Pfisterer (Eds.), Advances In Solar Energy Technology, Pergamon, Oxford, 1988, pp. 2999-3002.

[21] A.R. Dewit, D. Vanmaekelbergh, J.J. Kelly, A Study of the Photoanodic Dissolution of CdS With Electrical and Optoelectrical Impedance Spectroscopy, J. Electrochem. Soc. 139(9) (1992) 2508-2513.

[22] L.M. Peter, E.A. Ponomarev, D.J. Fermin, Intensity-modulated photocurrent spectroscopy: Reconciliation of phenomenological analysis with multistep electron transfer mechanisms, J. Electroanal. Chem. 427(1-2) (1997) 79-96.

[23] W.W. Gärtner, Depletion-Layer Photoeffects in Semiconductors, Physical Review 116 (1959) 84.

[24] L.M. Peter, Gurudayal, L.H. Wong, F.F. Abdi, Understanding the role of nanostructuring in photoelectrode performance for light-driven water splitting, J. Electroanal. Chem. 819 (2018) 447-458.

[25] F. Le Formal, E. Pastor, S.D. Tilley, C.A. Mesa, S.R. Pendlebury, M. Grätzel, J.R. Durrant, Rate Law Analysis of Water Oxidation on a Hematite Surface, J. Am. Chem. Soc. 137(20) (2015) 6629-6637.

[26] Y. Ma, C.A. Mesa, E. Pastor, A. Kafizas, L. Francàs, F. Le Formal, S.R. Pendlebury, J.R. Durrant, Rate Law Analysis of Water Oxidation and Hole Scavenging on a $BiVO_4$ Photoanode, ACS Energy Letters 1(3) (2016) 618-623.

[27] P.T. Landsberg, Recombination in Semiconductors, Cambridge University Press, Cambridge, 1991.

[28] D. Vanmaekelbergh, F. Cardon, Calculation of the electrical impedance associated with the surface recombination of free carriers at an illuminated semiconductor/electrolyte interface, J. Phys. D: Appl. Phys. 19(4) (1986) 643-656.

[29] M.M. Waegele, X. Chen, D.M. Herlihy, T. Cuk, How Surface Potential Determines the Kinetics of the First Hole Transfer of Photocatalytic Water Oxidation, J. Am. Chem. Soc. 136(30) (2014) 10632-10639.

[30] P. Allongue, H. Cachet, Band-Edge Shift amd Surface Charges at Illuminated n-GaAs Aqueous Electrolyte Junctions – Surface State Analysis and Simulation of their Occupation Rate, J. Electrochem. Soc. 132(1) (1985) 45-52.

[31] L.M. Peter, Semiconductor Electrochemistry, in: S. Giménez, J. Bisquert (Eds.), Photoelectrochemical Solar Fuel Production: From Basic Principles to Advanced Devices, Springer International Publishing, Cham, 2016, pp. 3-40.

[32] S.R. Pendlebury, M. Barroso, A.J. Cowan, K. Sivula, J.W. Tang, M. Grätzel, D. Klug, J.R. Durrant, Dynamics of photogenerated holes in nanocrystalline alpha-Fe_2O_3 electrodes for water oxidation probed by transient absorption spectroscopy, Chem. Commun. 47(2) (2011) 716-718.

[33] B.H. Erne, F. Ozanam, J.N. Chazalviel, The mechanism of hydrogen gas evolution on GaAs cathodes elucidated by in situ infrared spectroscopy, J. Phys. Chem. B 103(15) (1999) 2948-2962.

[34] J. Bisquert, V.S. Vikhrenko, Interpretation of the time constants measured by kinetic techniques in nanostructured semiconductor electrodes and dye- sensitized solar cells, J. Phys. Chem. B 108(7) (2004) 2313-2322.

[35] Q. Zhang et al., Density of Deep Trap States in Oriented TiO_2 Nanotube Arrays. J Phys. Chem. C 118 (2014) 18207-18213.

[36] C. Lohaus, A. Klein and W. Jaegermann, Limitation of Fermi level shifts by polaron defect states in hematite photoelectrodes. Nature Communications 9 (2018) 4309.

[37] A.G. Hufnagel, H. Hajiyani, S. Zhang, T. Li, O. Kasian, B. Gault, B. Breitbach, T. Bein, D. Fattakhova-Rohlfing, C. Scheu, R. Pentcheva, Why Tin-Doping Enhances the Efficiency of Hematite Photoanodes for Water Splitting—The Full Picture, Adv. Funct. Mater. 28(52) (2018) 1804472.